JOURNAL OF CATALYSIS 153, 304–316 (1995)

Total Oxidation of Carbon Monoxide and Methane over Transition Metal–Fluorite Oxide Composite Catalysts

I. Catalyst Composition and Activity

Wei Liu and Maria Flytzani-Stephanopoulos*,[1]

Department of Chemical Engineering, Massachusetts Institute of Technology, Cambridge, Massachusetts 02139; and
**Department of Chemical Engineering, Tufts University, Medford, Massachusetts 02155*

Received August 2, 1994; revised January 9, 1995

A novel metal oxide composite catalyst for the total oxidation of carbon monoxide and methane was prepared by combining fluorite oxides with active transition metals. The fluorite oxides, such as ceria and zirconia, are oxygen-ion-conducting materials having catalytic properties usually at high temperatures. Active base metal catalysts, such as copper, were used as additives to promote the catalytic properties of these oxides. The contact of the two types of materials gave rise to a high active oxidation catalyst. At a space velocity of about 42,000 h^{-1}, complete carbon monoxide oxidation in air occurred at room temperature on the $Au_{0.05}[Ce(La)]_{0.95}O_x$ catalyst and at ca. 100°C on Cu–Ce–O composite catalysts. At the same space velocity, total oxidation of methane on the Cu–Ce–O catalyst doped with La_2O_3 or SrO took place at ca. 550°C. The specific carbon monoxide oxidation activity of the Cu–Ce–O catalyst was several orders of magnitude higher than that of conventional copper-based catalysts and comparable or superior to platinum catalysts. This type of composite catalyst also showed excellent resistance to water vapor poisoning. The enhanced catalyst activity and stability resulted from strong interaction of the transition metal and fluorite oxide materials. © 1995 Academic Press, Inc.

1. INTRODUCTION

Carbon monoxide and gaseous hydrocarbons are ubiquitous air pollutants emitted by many sources. Complete oxidation of these pollutants to carbon dioxide and water over active catalysts is used to meet continually changing environmental regulations in an economic way. Precious metals (Pt, Pd) are well-known total oxidation catalysts with high activity and stability, and are widely used for exhaust gas emission control. The high cost of precious metals and their sensitivity to sulfur poisoning have long motivated the search for substitute catalysts. A variety of transition metal oxides and mixed metal oxides have been examined. However, base metal oxide catalysts are generally less active and stable in the presence of water vapor and sulfur compounds than the precious metal catalysts. Methane is the most refractory hydrocarbon and thus, is often used as model hydrocarbon compound for activity tests. In addition, methane itself is a potent greenhouse gas and the emission control of unburned methane from exhaust gases may be regulated in the future.

The fluorite-type oxides, such as ceria, zirconia, and thoria, have face-centered-cubic (FCC) crystal structure in which each tetravalent metal ion is surrounded by eight equivalent nearest O^{2-} ions forming the vertices of a cube. Oxygen vacancies are created when a fluorite oxide is doped by divalent or trivalent impurity ions. Thus, the fluorite oxides have been extensively studied as oxygen-ion-conducting materials (1, 2) due to their high oxygen vacancy concentration and mobility properties. In the catalysis field, fluorite oxides have been occasionally explored as catalysts for the oxidation of carbon monoxide and methane. CeO_2–La_2O_3, CeO_2–ThO_2, and UO_2–ThO_2 oxides were tested as carbon monoxide oxidation catalysts a long time ago (3–6). A redox mechanism involving lattice oxygen/oxygen vacancy participation was proposed for carbon monoxide oxidation on cerium oxide (7, 8). A recent atomic simulation of a carbon monoxide oxidation mechanism on cerium oxide (9) suggested that the surface oxygen of cerium oxide is more active than the bulk oxygen. Cerium oxide or zirconium oxide modified with other base metal oxides was tested for the oxidative coupling of methane (10, 11). For example, Ba-doped CeO_2 was found to be an active catalyst with high selectivity to C_2 species (11). Some other oxygen solid electrolytes, including Zr–Y–O, were examined for the total oxidation of carbon monoxide and methane from an electronic point of view (12). Typically, the fluorite-type oxides showed catalytic oxidation activity at high temperatures.

[1] To whom correspondence should be addressed.

0021-9517/95 $6.00

It is generally agreed that the oxidation of carbon monoxide and hydrocarbons over oxide catalysts involves surface oxygen/oxygen vacancy participation (7, 10, 11, 13, 14) and the oxygen mobility of metal oxide catalysts has something to do with catalytic activity. In our previous studies of the reduction of sulfur dioxide by carbon monoxide to elemental sulfur (15, 16), or, alternatively, the oxidation of carbon monoxide by sulfur dioxide, we found that cerium oxide and zirconium oxide are active catalysts. The oxidation of carbon monoxide by sulfur dioxide is considered to proceed via a redox mechanism involving surface oxygen/oxygen vacancy participation. The activity of cerium oxide for this reaction was enhanced by the addition of small amounts of rare earth oxide dopants (15). Further activity enhancement and catalyst resistance to water vapor and carbon dioxide poisoning were achieved by doping the fluorite oxide with transition metals, such as copper, cobalt, or nickel (16). Thus, we postulated that a general oxidation catalyst may be achieved by promoting fluorite oxides with active transition metals, such as copper. In such a catalyst configuration, the transition metals are used in minor amounts and stabilized in the fluorite oxide matrix, while the fluorite oxide is the essential and major catalyst component and not an inert support. We have found that this type of catalyst was highly active for the complete oxidation of carbon monoxide and methane in a preliminary study (17).

Cerium oxide has been widely used in the automotive three-way catalytic converter as an oxygen storage medium and thermal stabilizer. The interaction of ceria with precious metals (Pd, Pt, Rh) and its effect on catalytic activity have been intensively studied (18, 19). By contrast, little information is available to date on the interaction of fluorite oxides with base metal catalysts and their application to complete oxidation of carbon monoxide and methane. A recent paper (20) studied the effect of oxygen vacancies in yttria-stabilized zirconia (YSZ) support on the properties of copper catalyst for carbon monoxide oxidation. Several binary mixtures of transition metals and fluorite oxides have been proposed in the literature as methanol synthesis catalysts (21). However, an active catalyst for this application generally comprises the transition metal as the major component. From a materials point of view, alkaline earth and rare earth oxides have considerable solubility in fluorite oxides (22), while transition metal oxides have little or no solubility (23).

In the present study, we systematically examined the Cu–Ce–O composite oxide for carbon monoxide oxidation and the total oxidation of methane, and briefly surveyed some other transition metal–fluorite oxide systems. The reasons for the greater emphasis on the Cu–Ce–O systems are: (i) CeO_2 has a stable fluorite-type crystal structure from room temperature up to its melting point (2600°C); (ii) copper is known as an active oxidation catalyst; and (iii) both cerium and copper oxide precursors are readily available commercially.

2. EXPERIMENTAL

2.1. Catalyst Preparation

The bulk composite catalysts were prepared by coprecipitating aqueous salt solutions of the metals with ammonium carbonate or sodium carbonate. The ammonium carbonate was a good precipitation agent and did not introduce impurity metal ions, but the formation of metal–ammonia complex often caused some slippage of transition metals. If sodium carbonate was used, the precipitate had to be carefully washed to remove residual sodium. The precipitates were washed twice with hot deionized water and then dried for about 12 h at 110°C. The dried samples were typically heated for about 4 h at 650°C in air, unless specifically noted. Low purity (99%, Aldrich) cerium nitrate containing about 1.5 wt% lanthanum, corresponding to an atomic ratio of La to (La + Ce) of about 0.045, was used in the typical catalyst preparation. The cerium from this precursor was designated Ce(La) in the catalyst formula throughout the paper. High purity (99.99%, Aldrich) cerium nitrate was used to prepare the catalysts containing different dopant ions (Sr, Sc, La, Gd). Cerium acetate (99.9%, Aldrich), heated for 4 h at 750°C in air, was used as the primary precursor of La-free cerium oxide. Chloroauric acid ($HAuCl_4$), hydrogen hexachloroplatinate (IV) hydrate, and zirconium dichloride oxide hydrate were used as Au, Pt, and Zr precursors, respectively, while the AR grade metal nitrates were used for all other metals.

γ-Al_2O_3 was supplied by LaRoche. Bulk CuO was prepared by thermal decomposition of copper carbonate in air (4 h at 650°C). The supported catalysts were prepared by the conventional wet impregnation method using aqueous salt solutions of the metals. The slurry of the support and solution was degassed under vacuum so that the salt solution fully filled the pores of the support during impregnation. After excess solution was drained, the sample was dried for a few days at room temperature and then heated in air for 4 h at 650°C. The physical mixture of ceria and copper oxide, CuO + CeO_2, was prepared by blending the CuO and CeO_2 powders with water in an ultrasonic water bath for 10 min and followed by drying at 300°C for 1 h. For bulk composition analysis, the catalyst powder was dissolved in hydrofluoric acid and diluted with deionized water; the resulting solution was analyzed by inductively coupled plasma (ICP) atomic emission spectrometry (Perkin–Elmer Plasma 40). The catalyst surface composition was analyzed by X-ray photoelectron spectroscopy (XPS) on a Perkin–Elmer XPS 5100 system. The

catalyst characterization was performed by single-point desorption of nitrogen on a Micromeritics Flow Sorb II 2300 apparatus for BET surface area measurement and X-ray powder diffraction (XRD) on a Rigaku 300 X-ray diffractometer for crystalline phase identification. Throughout this paper, at.% denotes the ratio of a specific metal ion to the total metal ions in a given catalyst (×100%). The catalysts prepared by the coprecipitation and impregnation methods are denoted $Cu_x[Ce(La)]_{1-x}O_{2-\gamma}$ and CuO_x/CeO_2, respectively.

2.2. Apparatus and Procedure

Typically, catalysts were tested in a laboratory-scale packed-bed flow reactor consisting of a 0.6 cm i.d. × 50 cm long quartz tube with a porous quartz frit placed at the middle for supporting the catalyst. Occasionally, a 1.0 cm i.d. tube reactor was used when a large catalyst volume was needed. The reactor tube was heated by a Lindberg furnace. Flowing air was used to cool the outside surface of the reactor tube when the test was conducted at low temperatures (<100°C). The reaction temperature was monitored by a quartz-sheathed K-type thermocouple placed at the top of the packed catalyst bed and controlled by a Wizard temperature controller. CO and CH_4 reacting gases were certified calibration gas mixtures balanced by helium (from Matheson). Air and helium (all from AIRCO) were used as oxidizing gas and diluent, respectively. The gas streams were measured with rotameters and mixed prior to entering the reactor inlet. The resulting gas mixture flowed downward through the packed catalyst bed without further purification. Water vapor was introduced with helium bubbling through a heated water bath. The pressure drop of gas flowing through the assembly was small. Thus, experiments were carried out at nearly atmospheric pressure. The product gas stream was analyzed by a HP5880A gas chromatograph (GC) with a thermal conductivity detector (TCD). The carbon balance was checked by simultaneous measurement of the reactant and products. Unless specifically noted, the catalyst loading was 150 mg which resulted in a packed-bed height of typically 5 mm for CeO_2-based catalysts and 2–3 mm for ZrO_2-based catalysts in the 0.6 cm i.d. reactor. The total gas flow rate was set at 100 sccm consisting of 2% CO or 2% CH_4, 16% O_2, and the balance was He and N_2. Thus, the contact time was 0.09 g·s/cc(STP) and the space velocity was typically 42,000 h^{-1} for the CeO_2-based catalysts. The prepared catalysts were directly tested without any pretreatment unless specifically noted. The activity measurement was conducted in an ascending temperature manner so that the light-off behavior was recorded. No hysteresis effect was observed in these tests. The catalyst activity was ranked based on the light-off temperature at which 50% conversion occurred. The specific reaction rate was measured in differential reactor mode with conversion not exceeding 10% by choosing an appropriate catalyst loading and flow rate. The SiC powder was used as an inert mixer to keep approximately the same packing height when small amounts of the catalyst were tested.

3. RESULTS AND DISCUSSION

3.1. Carbon Monoxide Oxidation

3.1.1. CeO_2 and $Zr_{0.9}Y_{0.1}O_{1.9}$ catalysts. Figure 1 shows the light-off curves of CO oxidation over various CeO_2 catalysts containing different dopants as well as the $Zr_{0.9}Y_{0.1}O_{1.9}$ ($0.05Y_2O_3$-$0.9ZrO_2$) catalyst. The undoped CeO_2 had an activity similar to the La- and Sr-doped catalysts, but higher activity than the Sc- or Gd-doped catalysts. The $Zr_{0.9}Y_{0.1}O_{1.9}$ catalyst had an activity comparable to the CeO_2 catalysts at low temperatures and lower at high temperatures. In summary, all these catalysts showed relatively low activity with light-off temperatures (50% conversion) over the range of 360 to 440°C. According to the oxygen vacancy formation theory (24), one oxygen vacancy is created when one divalent (D^{2+}) or two trivalent (D^{3+}) dopant ions are introduced into fluorite crystal lattices. The resulting oxygen vacancy and the parent dopant ions are energetically associated pairs. The higher the association energy the lower the oxygen vacancy mobility. The association energies in CeO_2 doped with various alkaline or rare earth oxides were experimentally measured and calculated (24, 25). The association energy increases in the order Gd < La < Sc < Sr. The

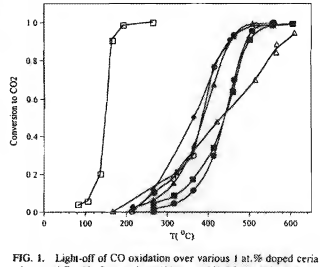

FIG. 1. Light-off of CO oxidation over various 1 at.% doped ceria catalysts and $Zr_{0.9}Y_{0.1}O_{1.9}$ catalyst (100 sccm: 2% CO, 16% O_2; surface areas: $Zr_{0.9}Y_{0.1}O_{1.9}$ = 42 m^2/g, 1 at.% Cu = 57 m^2/g, others ≅ 28 m^2/g); (□) Cu–[Ce(La)]O_2 prepared by 4-h heating in N_2 at 600°C; (◆) La; (▲) Sr; (○) no dopant; (■) Sc; (●) Gd; and (Δ) $Zr_{0.9}Y_{0.1}O_{1.9}$.

oxygen mobility in the doped CeO_2 catalysts was found to correlate well with the catalytic activity for the reduction of sulfur dioxide by CO (15), but the present activity results show that the activity of the doped CeO_2 catalysts for CO oxidation did not correlate with either the bulk oxygen vacancy concentration or oxygen mobility. In contrast to the alkaline earth and rare earth oxide dopants, 1 at.% Cu dopant significantly increased the catalytic activity of $[Ce(La)]O_2$ and lowered the light-off temperature to 135°C (Fig. 1). Thus, this catalyst was chosen for further study.

3.1.2. $Cu_{0.01}[Ce(La)]_{0.99}O_x$ catalyst. The fresh $Cu_{0.01}[Ce(La)]_{0.99}O_x$ catalyst shown in Fig. 1 was prepared by 4-h calcination at 600°C under N_2. This different calcination procedure was used in an attempt to keep copper ions inside the cerium oxide lattice, because copper oxide is immiscible with cerium oxide. However, further calcination of this catalyst in flowing air turned out to be beneficial to the catalyst activity. Figure 2 shows the light-off curve shifted to lower temperature after the catalyst was treated at higher temperature (660, 760, 860°C). But, the light-off curves converge at high conversions. Table 1 lists the catalyst surface area and surface composition after different thermal treatments. The catalyst surface was significantly enriched in copper as the heating temperature increased, while La was slightly enriched on the surface. The surface area decreased from the fresh value of 57 to 27.3 m^2/g after the catalyst was heated for 3 h at 860°C, while the light-off temperature (50% conversion) decreased from 150 to 80°C. These results show that copper oxide is not soluble in CeO_2, since calcining the catalyst in air drove the copper from the bulk to the surface, and the copper enrichment of the catalyst surface may have contributed to the activity increase. In contrast, the solubility of lanthanum oxide in cerium oxide was confirmed.

TABLE 1

Variation of the $Cu_{0.01}[Ce(La)]_{0.99}O_x$ Catalyst Surface Area and Surface Composition with Thermal Treatment in Air

Treatment	Surface area (m^2/g)	Composition (%)[a]		
		Cu	Ce	La
Fresh[b]	57.0	4.97	89.0	6.02
+3 h in flowing air at 650°C	52.4	8.10	86.5	5.37
+3 h in flowing air at 760°C	44.5	9.08	84.7	6.19
+3 h in flowing air at 860°C	27.3	11.90	81.4	6.74

[a] Determined by XPS with a standard deviation of ± 1%, but not calibrated.
[b] As prepared by 4-h calcination at 600°C in N_2.

3.1.3. $Cu_x[Ce(La)]_{1-x}O_{2-z}$ catalyst. Figure 3 shows the light-off curves over various bulk $Cu_x[Ce(La)]_{1-x}O_{2-z}$ catalysts prepared by coprecipitation. The experimental data for the catalysts with different bulk copper levels from 2 to 50 at.% are approximately represented by a single light-off curve, that is, the catalytic activity was not affected by the bulk copper content. The light-off temperatures were typically 80°C. Figure 4 shows the XRD patterns of these catalysts. At low copper content, there were no visible peaks due to the CuO crystal phase. As the copper content increased, the CuO peaks became apparent. We also see that the CuO peak width is generally narrower than that of the CeO_2 peak, although the inten-

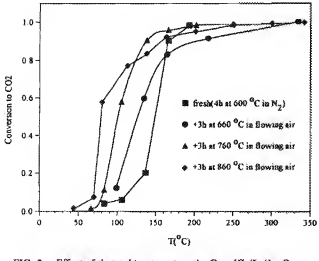

FIG. 2. Effect of thermal treatment on the $Cu_{0.01}[Ce(La)]_{0.99}O_x$ catalyst activity for CO oxidation (100 sccm: 2% CO, 16% O_2).

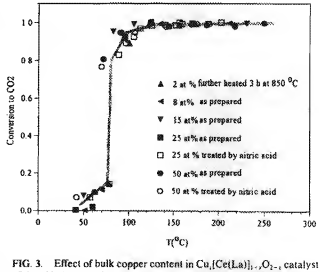

FIG. 3. Effect of bulk copper content in $Cu_x[Ce(La)]_{1-x}O_{2-z}$ catalyst on CO oxidation activity (100 sccm: 2% CO, 16% O_2; surface areas = 30 m^2/g).

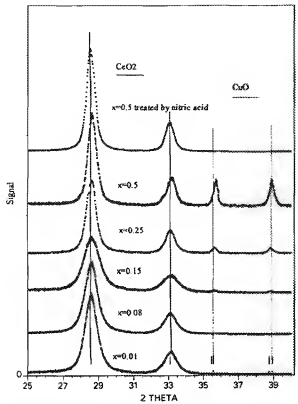

FIG. 4. XRD pattern of the Cu–Ce(La)–O catalysts ($K\alpha_1$ copper radiation, 50 kV, 200 mA, scan rate 1°/min).

sity of the CuO peak is smaller. The crystal particle sizes of CuO and CeO_2 were estimated by peak broadening (26) with Scherrer's equation and are listed in Table 2. Table 2 also lists the surface composition determined by XPS. It is interesting that at low bulk copper content the surface copper content was higher than the bulk average, but the surface copper no longer increased for bulk copper contents higher than ca. 15 at.%. It appears that copper is finely dispersed in CeO_2 at low copper contents, and when saturation is reached at higher copper contents, the excess copper formed bulk CuO particles that do not contribute to the XPS signal (or "invisible" to XPS).

On the basis of the activity results, we propose that the catalyst activity derives primarily from the combination of finely dispersed copper–cerium oxide system, while the CuO particles have negligible contribution. This hypothesis was confirmed by the following experiment. Bulk CuO can be easily dissolved in nitric acid. Thus, the bulk CuO particles in the $Cu_x[Ce(La)]_{1-x}O_{2-x}$ catalyst were removed by immersing the sample in nitric acid for 14 h and then filtering, washing with deionized water, and drying at 650°C for 1 h. The catalyst compositions after this treatment are shown in Table 2. The higher the initial bulk copper content the more copper was removed by this process resulting in similar bulk composition (as determined by ICP) for three copper-containing catalysts: 15, 25, and 50 at.%, in spite of large initial composition differences. XRD analyses of the nitric-acid-treated catalysts revealed the absence of the CuO phase as shown in Fig. 4. The surface composition of the treated 50 at.% Cu catalyst is similar to the 2 at.% Cu catalyst. Figure 3 shows a negligible difference in the catalytic activities between the fresh and the nitric-acid-treated catalysts. Thus, we conclude that copper clusters, invisible by XRD and stabilized by strong interaction with CeO_2, mainly contribute to the catalytic activity. Only a small amount of copper (a few percent) is needed to promote the CO

TABLE 2

Particle Size and Surface Composition of Cu–Ce(La)–O Catalysts

Catalyst	Particle size (nm)[a]		Surface composition (%)[b]		
Cu/(Cu + Ce) × 100%	CeO_2	CuO	La	Cu	Ce
2[c]	10	—	5.9	11.7	82.4
8(6)[d]	10	—	5.97	16.2	77.8
15(10.5)[d]	7.6	—	3.42	24.8	71.7
25(8.4)[d]	13	29	5.91	18.7	75.4
50(8.8)[d]	14(14)[d]	29	5.8(6.9)[d]	18.9(11.4)[d]	75.3(81.7)[d]

[a] CeO_2 and CuO particle sizes were determined by XRD from the (111) and ($\bar{1}$11) peak widths at half maximum of CeO_2 and CuO, respectively.

[b] Determined by XPS with a standard deviation of ±1%, but not calibrated.

[c] Prepared by 4-h calcination at 650°C plus 3-h calcination at 860°C both in air.

[d] The sample was immersed in nitric acid for 14 h at room temperature, filtered, washed with deionized water, and dried for 1 h at 650°C.

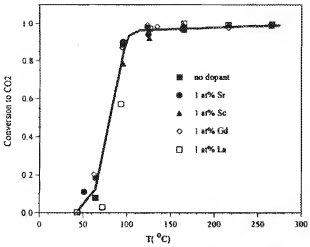

FIG. 5. Effect of 1 at.% dopant on the CO oxidation activity of $Cu_{0.15}Ce_{0.85}O_x$ catalyst (100 sccm: 2% CO, 16% O_2; surface areas ≈ 30 m^2/g).

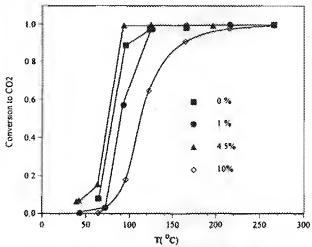

FIG. 6. Effect of La dopant content on the CO oxidation activity of $Cu_{0.15}Ce_{0.85}O_x$ catalyst (100 sccm: 2% CO, 16% O_2; surface areas ≈ 30 m^2/g).

oxidation activity of CeO_2, and excess copper forms bulk CuO particles contributing little to the catalyst activity. The bulk copper content needed for uniform surface coverage of a CeO_2 catalyst with a 30 m^2/g surface area was calculated to be 8.5 at.% by assuming monolayer Cu^{2+} ions of radius equal to 0.07 nm. This fact and the surface compositions listed in Tables 1 and 2 suggest that only a small fraction of copper in the Cu–Ce–O catalyst of high copper content is dispersed on the cerium oxide surface. Further details of the catalyst microstructure are given in Part II of this paper (27).

3.1.4. Effect of dopant oxides on the catalytic activity of $Cu_{0.15}Ce_{0.85}O_x$ catalyst. The effect of 1 at.% alkaline earth or rare earth dopant oxide on the CO oxidation activity of the $Cu_{0.15}Ce_{0.85}O_x$ catalyst is shown in Fig. 5. The light-off curves on all the catalysts virtually overlapped. It seems that 1 at.% dopant (La, Sr, Gd) had little effect on the CO oxidation activity of the $Cu_{0.15}Ce_{0.85}O_x$ catalyst, similar to the case of the bulk CeO_2 catalyst (Fig. 1). The effect of La dopant content on the $Cu_{0.15}Ce_{0.85}O_x$ catalyst activity is shown in Fig. 6. La dopant had a negative effect on the catalytic activity when its doping level reached 10 at%. The surface La content of this catalyst was about 18 at.%. Thus, the activity decrease may be due to excessive La enrichment of the catalyst surface. The variation in the activity at low La-doping levels was probably caused by some variability in catalyst preparation. Typically, the activity measurement showed good reproducibility, while the catalyst preparation by coprecipitation had fair reproducibility with about ±10°C variation in the light-off temperature. It is also noted that Na impurity introduced in the coprecipitation with sodium carbonate had an adverse effect on the catalytic activity. However, the catalysts prepared with ammonium carbonate and sodium carbonate showed similar activity as long as the Na ions were carefully washed away.

3.1.5. Activity enhancement by the concerted effect of CuO and CeO_2. The experimental results presented thus far have indicated that the Cu–Ce–O type mixed oxide is a highly active catalyst for CO oxidation, as full conversion to CO_2 over this catalyst occurred around 100°C. The catalyst activity is due to the synergistic effect between CuO and CeO_2 as illustrated by Fig. 7. Bulk CeO_2

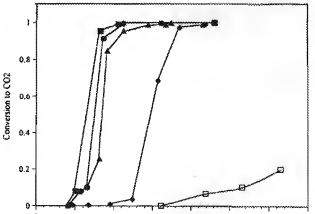

FIG. 7. Activity enhancement for CO oxidation from combination of CeO_2 and CuO (100 sccm: 2% CO, 16% O_2): (■) $Cu_{0.15}[Ce(La)]_{0.85}O_x$, 30 m^2/g; (●) 15 at.% CuO_x/CeO_x, 22.4 m^2/g; (▲) 15 at.% CuO + CeO_2 prepared by 1-h heating in air at 300°C, 18.6 m^2/g; (◆) bulk CuO, 1.64 m^2/g; (□) CeO_2, 28 m^2/g.

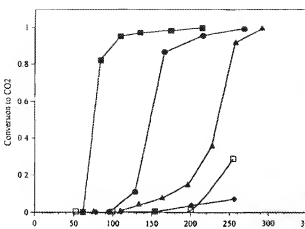

FIG. 8. Effect of copper dispersion on CO oxidation activity (100 sccm: 2% CO, 16% O_2); (■) $Cu_{0.15}[Ce(La)]_{0.85}O_x$, 50 mg, 30 m^2/g; (●) CuO, 1000 mg, 1.64 m^2/g; (▲) 14 at.% CuO/γ-alumina, 150 mg, 137 m^2/g; (◆) 3.2 at.% Cu-ZSM-5, 150 mg, 400 m^2/g; (□) 3.1 at.% Ce, 1 at.% Cu, Ce–Cu–ZSM-5, 150 mg, 400 m^2/g.

catalyst had low activity at low temperatures, while bulk CuO is known as an active catalyst for CO oxidation with a light-off temperature (50% conversion) around 140°C as measured in this work. When the same bulk CuO powder was mixed with the CeO_2 powder with an atomic ratio of 15 : 85 according to the procedure described earlier, the light-off curve shifted to lower temperatures by about 80°C. The 15 at.% Cu-containing bulk catalyst $Cu_{0.15}[Ce(La)]_{0.85}O_x$ and the impregnated 15 at.% CuO_x/CeO_2 catalysts showed only slightly higher activity than the physical mixture.

The bulk CuO had much lower surface area than the Cu–Ce–O catalyst. To clarify that the activity enhancement effect was due to the interaction of CuO and CeO_2, additional tests were run, as shown in Fig. 8. The light-off curves on the $Cu_{0.15}[Ce(La)]_{0.85}O_x$ and bulk CuO catalysts in Fig. 8 were measured on the basis of the same total BET surface area. The light-off temperature on the $Cu_{0.15}[Ce(La)]_{0.85}O_x$ catalyst was still about 70°C lower than that on the bulk CuO. Compared to Fig. 7, the light-off curve on the bulk CuO catalyst was not affected as the CuO loading increased from 150 to 1000 mg. The 14 at.% CuO/γ-Al_2O_3 catalyst had significantly lower activity than the bulk CuO, but comparable activity to catalysts reported in the literature. This may be explained by the known formation of copper aluminate in alumina-supported copper oxide catalyst. The specific copper surface area of this catalyst measured by N_2O decomposition was about 50 m^2/g. The copper dispersion effect was also examined in Fig. 8 with 3.2 at.% Cu–ZSM-5 and 3.1 at.% Ce plus 1 at.% Cu, Ce–Cu–ZSM-5 catalysts. Compared to the 2 at.% Cu-containing Cu–Ce(La)–O catalysts (Fig. 3), these ion-exchanged zeolite catalysts had very low activity at temperatures lower than 250°C. Copper dispersion in these two catalysts, however, is high, because copper ions are associated with Al ions in the ZSM-5 framework (28). The results in Figs. 7 and 8 clearly indicate that the Cu–Ce–O catalyst has much higher activity than other copper-based catalysts on the basis of either unit catalyst weight or total surface area. While good metal dispersion is, in general, necessary to obtain an active catalyst, high copper dispersion alone is not sufficient to achieve an active CO oxidation catalyst; the enhanced activity of the Cu–Ce–O composite catalyst must result from the interaction of copper and CeO_2 or a "concerted effect" between these two kinds of materials.

The reaction rate on the $Cu_{0.15}[Ce(La)]_{0.85}O_x$ catalyst is compared with those on some well-known CO oxidation catalysts reported in the literature (29–31) in Table 3. Manganese-based mixed oxides have long been known as low temperature CO oxidation catalysts. Copper oxide is also one of the most studied oxidation catalysts. The reaction rate on the $Cu_{0.15}[Ce(La)]_{0.85}O_x$ is a few times higher than that on the Mn-based catalysts and 300 times higher than on the Cu/δ-alumina catalyst. Recently, Rajadurai and Carberry (31) reported the perovskite-type mixed oxide, $La_{0.8}Sr_{0.2}CrO_{3-\delta}$, as an active CO oxidation catalyst rivaling the platinum catalysts. Table 3 shows that $Cu_{0.15}[Ce(La)]_{0.85}O_x$ has a reaction rate per unit catalyst weight comparable to that of the Pt/alumina catalyst and much higher than that of $La_{0.8}Sr_{0.2}CrO_{3-\delta}$. The conventional N_2O decomposition method (32) was tried to measure the specific copper surface area in the Cu–Ce(La)–O catalyst. However, we were not able to get a reliable measurement due to the strong interaction between Cu and $[Ce(La)]O_2$. The specific copper surface area in the $Cu_{0.15}[Ce(La)]_{0.85}O_x$ catalyst was roughly estimated by multiplying the BET surface area by the surface atomic fraction of copper in Table 2. Table 3 shows that the specific reaction rate on the $Cu_{0.15}[Ce(La)]_{0.85}O_x$ is comparable to the Pt/alumina and the $La_{0.8}Sr_{0.2}CrO_{3-\delta}$. Therefore, the Cu–Ce–O system has both low light-off temperatures and high intrinsic activity for CO oxidation.

3.1.6. Activities of other transition metal–fluorite oxide catalysts. So far we have considered the Cu–Ce(*D*)–O system where *D* denotes a dopant element. Next, the CO oxidation over other transition metal–fluorite oxide systems will be briefly discussed. Several light-off curves are shown in Fig. 9. The $Au_{0.05}[Ce(La)]_{0.95}O_x$ catalyst prepared by calcination in air for 1 h at 500°C followed by 1 h at 600°C exhibited the highest activity. Complete CO oxidation over this catalyst occurred at room temperature (26°C). Pt–Ce(La)–O, Cu–Zr–O, and Cu–Zr(Y)–O catalysts showed comparable activity, slightly higher than the Co–Ce(La)–O catalyst, but all these catalysts, except for

TABLE 3

Catalyst Activity for CO Oxidation

Catalyst and Reaction Condition	Surface area (m^2/g)	Rate (μmol/gcat · s)[a]	Rate (μmol/m^2 · s)[b]
I. P_{CO} = 0.01 bar, 130°C			
$Cu_{0.15}[Ce(La)]_{0.85}O_x$[c]	30	85	2.8
Amorphous $CuMnO_x$ (28)[d]	39	10	0.27
II. P_{CO} = 0.01 bar, 80°C			
$Cu_{0.15}[Ce(La)]_{0.85}O_x$[c]	30	19	0.63
Spinel $CoCuMnO_4$ (28)[d]	113	9.4	0.083
III. P_{CO} = 0.035 bar, 130°C			
$Cu_{0.15}[Ce(La)]_{0.85}O_x$[c]	30	195	6.5
12 wt% Cu/δ-alumina (30)[e]	138	0.64	0.005
IV. P_{CO} = 0.01 bar, 110°C			
$Cu_{0.15}[Ce(La)]_{0.85}O_x$[c]	30	32	1.1(4.3)[f]
0.5 wt% Pt/alumina (31)[f]	247	25	0.10(5.5)[f]
$La_{0.8}Sr_{0.2}CrO_{3-\delta}$ (31)[f]	0.33	1.8	5.5

[a] Specific rate based on unit catalyst weight.
[b] Specific rate based on unit BET surface area.
[c] Partial pressure of oxygen, P_{O_2} is 0.17 bar.
[d] P_{O_2} = 0.2 bar.
[e] Specific rate based on specific copper or platinum surface area. The specific copper surface area was estimated by BET area × surface copper fraction (Cu/(Cu + La + Ce)).
[f] 1% CO, 99% O_2, unknown total pressure.

Au–Ce(La)–O, were less active than the Cu–Ce(La)–O catalyst. Fine gold particles supported on Co_3O_4, α-Fe_2O_3, and TiO_2 were found to be excellent low temperature CO oxidation catalysts by Haruta *et al.* (33). The high activity was considered to be due to active catalytic sites formed at the boundary of gold particle and metal oxide where CO adsorbed on gold reacted with the oxygen adsorbed on the metal oxide. The activity of the present $Au_{0.05}[Ce(La)]_{0.95}O_x$ catalyst was compared with the Au/α-Fe_2O_3 in Table 4. The activity of the $Au_{0.05}[Ce(La)]_{0.95}O_x$ catalyst was slightly lower than that of the Au/α-Fe_2O_3, which may be due to the larger gold particle size in the $Au_{0.05}[Ce(La)]_{0.95}O_x$ catalyst. In contrast to the Cu–Ce(La)–O system where finely dispersed copper cannot be dissolved in nitric or hydrochloric acid due to the strong interaction with cerium oxide, the gold particles in the $Au_{0.05}[Ce(La)]_{0.95}O_x$ catalyst can be dissolved in hydrochloric acid, while bulk gold is insoluble. This implies that the small gold particles in the $[Ce(La)]O_x$ matrix indeed have some particular properties. It is noteworthy that the $Au_{0.05}[Ce(La)]_{0.95}O_x$ catalyst showed good stability. The catalyst maintained its high activity after being subjected to a 3-h treatment at 650°C either in flowing air or 25% H_2/He. No deactivation was observed in a 4-day run at room temperature with the reacting gas saturated with water vapor. The water vapor effect on the other catalysts is addressed in the following section.

3.1.7. Effect of water vapor on catalyst activity. Water vapor generally inhibits or poisons the oxidation activity of base metal oxide catalysts and imposes a second challenge beyond that of boosting the activity of the non-precious metal oxide catalysts. The extensive search of

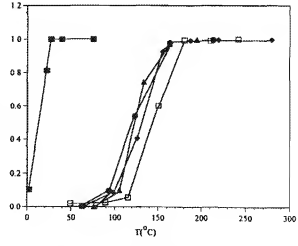

FIG. 9. CO oxidation over various composite catalysts (150 mg catalyst loading; 100 sccm: 2% CO, 16% O_2); (■) $Au_{0.05}[Ce(La)]_{0.95}O_x$ prepared by air calcination for 1 h at 500°C + 1 h at 600°C, 34.2 m^2/g; (●)$Pt_{0.05}[Ce(La)]_{0.95}O_x$, 28.1 m^2/g; (▲) $Cu_{0.2}Zr_{0.4}O_x$, 17.8 m^2/g (◆) $Cu_{0.15}[Zr_{0.9}Y_{0.1}]_{0.85}O_x$, 65 m^2/g; (□) $Co_{0.2}[Ce(La)]_{0.8}O_x$, 30 m^2/g.

TABLE 4

Gold–Metal Oxide Composite Catalyst Activity for CO Oxidation

Catalyst	Surface area (m^2/g)	Au particle size (nm)	Rate at 31°C (μmol/gcat · s)[a]
$Au_{0.01}[Ce(La)]_{0.99}O_x$	34.2	8.0	1.2
5 at.% Au/α-Fe_2O_3 (33)	72.0	4.0	1.9

[a] Rate calculated based on formation of CO_2 under the conditions of 1% CO, 1% O_2.

base metal catalysts as alternatives to precious metals for exhaust gas treatment in the 1960s identified copper oxide, mixed with chromium oxide and/or rare earth oxides, to be an active catalyst (34, 35). However, the copper catalyst was severely deactivated upon addition of water vapor due to changes in the nature of surface copper (36). Perovskite-like compounds $RE_{1-x}Pb_xMnO_3$ and $RECoO_3$ (RE = La, Pr, or Nd) were pioneered as oxidation catalysts for the automotive exhaust treatment in the early 1970s (37). Although these mixed oxides later showed a lower activity than the precious metal catalyst and a propensity to water vapor poisoning (38, 39), they have indeed stimulated intensive studies of this type of catalyst.

The water vapor effect on the present catalysts was examined and typical results are shown in Fig. 10. Water vapor effects on the bulk CuO and the 14 at.% CuO/γ-Al_2O_3 catalysts are also included in Fig. 10 for comparison. The water vapor content in exhaust gas streams is

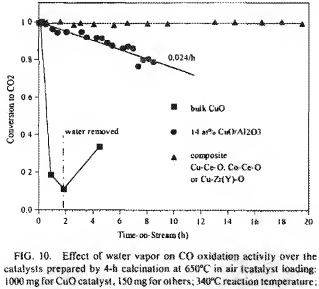

FIG. 10. Effect of water vapor on CO oxidation activity over the catalysts prepared by 4-h calcination at 650°C in air (catalyst loading: 1000 mg for CuO catalyst, 150 mg for others; 340°C reaction temperature; 47 sccm H_2O + 100 sccm dry gas containing 2% CO and 16% O_2).

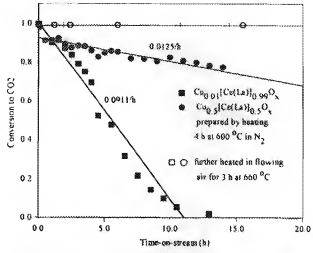

FIG. 11. Effect of catalyst thermal treatment on the CO oxidation activity in the presence of water vapor (150 mg catalyst loading; 340°C reaction temperature; 47 sccm H_2O + 100 sccm dry gas containing 2% CO and 16% O_2).

usually around 15%. Excess water vapor, 32%, was used in our tests to study its effect. In Fig. 10, the CO conversion on the bulk CuO catalyst decreased to 0.1 from 0.99 within about 2 h after the addition of water vapor at 340°C. The conversion recovered to only 0.35 2 h after the reacting gas was switched back to the dry gas feed stream. The conversion over the CuO/γ-Al_2O_3 catalyst also decreased monotonically at a rate of about 0.03/h in the presence of water vapor. In contrast, no deactivation was observed over the Cu–Ce(La)–O, Co–Ce(La)–O, and Cu–Zr(Y)–O catalysts under the same experimental conditions. It is noted that the preceding calcination process during catalyst preparation had a strong effect on the Cu–Ce(La)–O catalyst activity in the presence of water vapor as illustrated in Fig. 11. On the $Cu_{0.01}[Ce(La)]_{0.99}O_x$ and $Cu_{0.5}[Ce(La)]_{0.5}O_x$ catalysts prepared by 4 h-calcination at 600°C under N_2, the conversion declined monotonically at a rate of about 0.09/h and 0.012/h, respectively. However, these two catalysts maintained stable activity in the presence of water vapor after they were further heated for 3 h at 650°C in flowing air.

In conclusion, the transition metal–fluorite oxide composite catalyst exhibits significant enhancement for carbon monoxide oxidation in both catalytic activity and stability in the presence of water vapor, and the enhancement stems from the strong interaction of the two kinds of materials.

3.2. Methane Oxidation

Screening tests for total methane oxidation were performed over several transition metal–fluorite oxide cata-

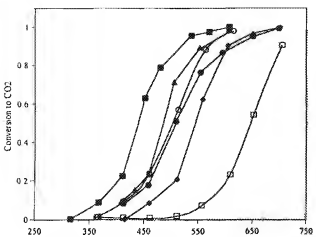

FIG. 12. Methane oxidation over various composite catalysts (150 mg catalyst loading; 100 sccm: 2% CH_4, 16% O_2). (■) $Cu_{0.2}Zr_{0.8}O_x$, 17.8 m^2/g; (▲) $Cu_{0.08}[Ce(La)]_{0.92}O_x$, 43 m^2/g; (○) $Cu_{0.3}[Ce(La)]_{0.7}O_x$, 27.8 m^2/g; (●) $Cu_{0.5}Zr_{0.5}O_x$, 50.0 m^2/g; (◆) $[Ce(La)]O_2$, 30 m^2/g; (□) CeO_2, 28 m^2/g.

lysts at a contact time of 0.09 g · s/cc (STP). ZrO_2-based catalysts prepared in this work had much higher packing density than the CeO_2-based catalysts. The space velocity for the ZrO_2-based catalysts was about 100,000 h^{-1}, while the space velocity for the CeO_2-based catalysts was typically 42,000 h^{-1}. In Fig. 12, the $Cu_{0.2}Zr_{0.8}O_x$ catalyst showed high activity for methane oxidation with a light-off temperature (50% conversion) at 450°C. The $Cu_{0.3}Zr_{0.3}O_x$ catalyst had a light-off temperature of 510°C, which suggests that an excessive amount of copper in the Cu–Zr–O catalyst system may have a negative effect on catalytic activity. Bulk CeO_2 had the lowest activity among the catalysts tested. However, the light-off temperature over CeO_2 was lowered from 650 to 540°C in the presence of 4.5 at.% La dopant and further to 490°C by the addition of 8 at.% Cu. The 50 at.% Cu-containing Cu–Ce(La)–O catalyst showed similar activity to the one containing 8 at.% Cu.

The 15 at.% Cu-containing Cu–Ce(D)–O catalysts with different dopants were examined and the results are shown in Fig. 13. The 1 at.% Sc-doped $Cu_{0.15}Ce_{0.85}O_x$ catalyst had slightly higher activity than the undoped one, while the 1 at.% La-doped or 1 at.% Sr-doped catalyst had significantly higher activity than the undoped. The 4.5 at.% La-doped catalyst, $Cu_{0.15}[Ce(La)]_{0.85}O_x$, had the highest activity, but further increasing the La dopant level to 10 at.% decreased the catalytic activity, which was similar to the case of CO oxidation. Methane conversions to carbon dioxide of 50 and 95% over the $Cu_{0.15}[Ce(La)]_{0.85}O_x$ took place at 450 and 520°C, respectively. The $Cu_{0.15}[Ce(La)]_{0.85}O_x$ showed comparable activity to the $Cu_{0.2}Zr_{0.8}O_x$ catalyst in Fig. 12 and higher activity than $Cu_{0.08}[Ce(La)]_{0.92}O_x$ or $Cu_{0.3}[Ce(La)]_{0.7}O_x$ in Fig. 12. The activity of the $Cu_{0.15}[Ce(La)]_{0.85}O_x$ catalyst was stable as no conversion decline was observed during a 15-h run at 600°C with 99% methane conversion. Therefore, the dopant oxide in the CeO_2-based catalyst played a more important role in methane oxidation than in CO oxidation. However, the activity enhancement cannot be explained simply on the basis of oxygen vacancy and energetics. SrO and La_2O_3 are more basic oxides than Sc_2O_3. It is plausible to assume that the catalyst surface acidic/basic sites are important for methane oxidation. This assumption is illustrated by the following reaction scheme where "cat" denotes the catalyst, M^{n+} is an acidic site, and O^- is a basic site:

$$M^{n+}_{cat}\text{–}CH_3^{\delta-} \cdots H^{\delta+}\text{–}O^-_{cat} \xrightarrow{slow} M^{n+}_{cat}\text{–}CH_3^- + HO_{cat}.$$

It is generally agreed that the most difficult step in activating methane is to break the C–H bond (10, 40). As one hydrogen atom is abstracted from the methane molecule by a surface oxygen (basic site), the negatively charged residual is stabilized by a surface acidic site. The resulting intermediate can become a methyl radical by giving back its electron to the catalyst and the methyl radical may subsequently form the precursors of a variety of chemical products. These intermediate species are easily oxidized into carbon dioxide and water. Both surface basic and acidic sites with suitable strength and geometry are needed to form a transition state and lower the activation energy in the C–H bond breakage. The present results indicate that copper–fluorite oxide composites are active

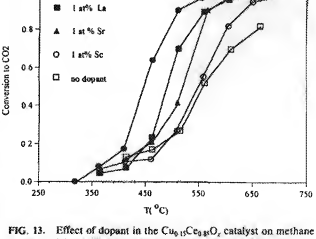

FIG. 13. Effect of dopant in the $Cu_{0.15}Ce_{0.85}O_x$ catalyst on methane oxidation activity; (150 mg catalyst loading; catalyst surface area = 30 m^2/g; 100 sccm: containing 2% CH_4 and 16% O_2).

TABLE 5

Catalyst Activity for Methane Oxidation

Catalyst and reaction condition	Surface area (m^2/g)	Rate[a] (μmol/gcat · s)	Rate[a] (μmol/m^2 · s)
I. P_{CH_4} = 0.01 bar, P_o = 0.04 bar, 557°C			
$Cu_{0.15}[Ce(La)]_{0.85}O_x$[b]	30	11	0.36
$LaCoO_3$ (41)	3.5	1.3	0.36
II. P_{CH_4} = 0.04 bar, 550°C			
$Cu_{0.15}[Ce(La)]_{0.85}O_x$[b]	30	48	1.6
$La_{0.95}Sr_{0.05}Ni_{0.3}Co_{0.7}O_3$ (42)[c]	19	11	0.60
$La_{0.9}Sr_{0.1}MnO_3$ (43)[c]	—	6.6	—

[a] Rate calculated based on CO_2 formation.
[b] Partial pressure of oxygen, P_{O_2}, is 0.12 bar.
[c] P_{O_2} = 0.2 bar.

catalysts for methane oxidation and more importantly, the activity is tunable by using different dopant oxides in suitable amounts.

It is noted that methane oxidation is much slower than carbon monoxide oxidation, and the light-off curves shown in Figs. 12 and 13 are in the kinetic regime; that is, the light-off curve will be shifted to lower temperatures by increasing the contact time. Table 5 briefly compares the activity of the $Cu_{0.15}[Ce(La)]_{0.85}O_x$ catalyst with some active perovskite mixed oxide catalysts reported in the literature (41–43). Per unit catalyst weight, the $Cu_{0.15}[Ce(La)]_{0.85}O_x$ catalyst had an activity a few times higher than that of the other catalysts. Per unit surface area, the activity of the $Cu_{0.15}[Ce(La)]_{0.85}O_x$ catalyst was comparable to that of the $LaCoO_3$ catalyst, an extensively studied perovskite system. Formation of the perovskite compound requires a high temperature so that it is difficult to prepare with a high surface area. The preparation of the present transition metal–fluorite oxide composite catalyst mostly requires good dispersion of the transition metals in the fluorite matrix and thus, a high catalyst surface area can be obtained by using appropriate low temperature synthesis methods. In conclusion, the present composite oxide catalyst is a promising new catalyst system showing high activity for the total oxidation of methane.

3.3. Simultaneous Oxidation of CO and CH_4 over the $Cu_{0.15}[Ce(La)]_{0.85}O_x$ Catalyst

Figure 14 shows the light-off curves of carbon monoxide and methane oxidation over the $Cu_{0.15}[Ce(La)]_{0.85}O_x$ catalyst in two different reacting gas mixtures. The oxidizing gas (II) consisted of 0.228% CH_4, 0.1% CO, and 1.0% O_2. The reducing gas composition (III) consisted of 0.228% CH_4, 0.1% CO, and 0.35% O_2. The light-off curves under the oxidizing and reducing conditions overlapped, and the light-off curves of methane oxidation in the presence of CO were similar to light-off in the absence of CO. There was 95% conversion of CO and methane at about 100 and 550°C, respectively. The oxidation behavior of the present catalyst is very different from that on precious metal catalysts (Pd, Pt, Rh) reported in the literature (44). On the precious metal catalysts, the light-off curves of both CO oxidation and CH_4 oxidation were strongly affected by the reacting atmosphere. Under reducing conditions, methane oxidation produced substantial amounts of CO and H_2 at high temperatures (44), while no partial oxidation products (CO, H_2) were observed over the present catalyst. This was confirmed by separate studies at vari-

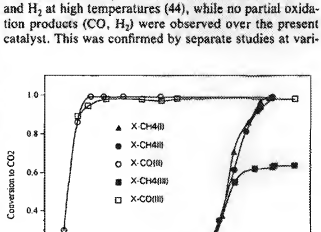

FIG. 14. Simultaneous oxidation of methane and CO over the $Cu_{0.15}[Ce(La)]_{0.85}O_x$ catalyst. (I) in 0.228% CH_4, 1% O_2; (II) in oxidizing gas containing 0.228% CH_4, 0.1% CO, 1% O_2; and (III) in reducing gas containing 0.228% CH_4, 0.1% CO, 0.35% O_2.

ous space velocities. The CO and H_2 oxidation on the metal–fluorite oxide composite catalysts appear to proceed very quickly, as previously noted. This is an advantage of the present catalyst over the precious metal catalysts, because CO is a more harmful pollutant than methane.

4. SUMMARY

Transition metal–fluorite oxide composite catalysts were studied in this work for the total oxidation of carbon monoxide and methane. A variety of highly active oxidation catalysts can be prepared from this family of catalysts. The transition metal or metal oxide is usually insoluble in the fluorite oxide, while alkaline earth and rare earth oxides have solubility over a wide concentration range. Therefore, transition metals can be well dispersed in the fluorite oxide matrix without one worrying about the adverse effect of solid solution formation, and alkaline and rare earth oxide can be used to tune the physical and chemical properties of the fluorite oxides. The good transition metal dispersion and, more importantly, the strong interaction between the transition metal and the fluorite oxide result in high catalyst activity and stability. The transition metal dispersion and display of this strong interaction are not sensitive to the catalyst preparation process. Some specific conclusions were drawn from this work as follows:

4.1 Carbon Monoxide Oxidation

(1) The Cu–Ce–O composite showed higher CO oxidation activity than that of any other of the base metal oxide catalysts reported in the literature. The catalytic activity was not affected by small amounts of alkaline earth and rare earth dopants or impurities (ca. 1 at.%). Only a small amount of copper (ca. 2 at.% or 0.7 wt%) was needed to promote the catalytic activity of CeO_2, while excess copper formed bulk CuO particles contributing little to the catalyst activity. These catalysts showed excellent resistance to water vapor poisoning.

(2) The $Au_{0.01}[Ce(La)]_{0.99}O_y$ is an active and stable catalyst for low temperature CO oxidation (room temperature).

(3) The activity of the Cu–Ce–O system was superior to Co–Ce–O and Cu–Zr–O, but all these catalyst systems showed good resistance to water vapor poisoning.

4.2 Methane Oxidation

(4) The Cu–Ce–O and Cu–Zr–O composites are active catalysts for the total oxidation of methane. The Cu–Ce–O catalyst activity can be tuned by using alkaline earth and rare earth oxide dopants in suitable amounts. Both La and Sr dopants provided significant promotion effect.

(5) No partial oxidation products, such as CO and H_2, were observed during methane oxidation over the Cu–Ce(La)–O and Cu–Zr–O catalysts under reducing conditions.

Further characterization of the Cu–Ce(La)–O catalyst and CO and methane oxidation kinetics will be presented in Part II of this paper (27).

ACKNOWLEDGMENTS

This work has been supported by the U.S. Department of Energy, University Coal Research Program under Grant DE-FG22-92PC92534. The authors thank Dr. A. Tschoepe for his assistance in the surface area measurements, Mr. Y. P. Zhang for supplying the Cu–ZSM-5 catalysts, and the reviewers of this manuscript for their comments. This work made use of MRSEC Shared Facilities supported by the National Science Foundation under Award DMR-9400334.

REFERENCES

1. Tuller, H. L., and Moon, P. K., *Mater. Sci. Engl. B* **1**, 171 (1988).
2. Hagenmuller, P., and Van Gool, W., "Solid Electrolytes." Academic Press, New York, 1978.
3. RienAcker, G., *Z. Anorg. Allg. Chem.* **259**, 280 (1949).
4. RienAcker, G., and Wu, Y., *Z. Anorg. Allg. Chem.* **315**, 121 (1962).
5. RienAcker, G., and Birckenstaedt, M., *Z. Anorg. Allg. Chem.* **262**, 81 (1950).
6. Claudel, B. M., and Brau, G. G., *J. Catal.* **14**, 322 (1969).
7. Breysse, M., Guenin, M., Claudel, B., Latreille, H., and Veron, J., *J. Catal.* **27**, 275 (1972).
8. Breysse, M., Guenin, M., Claudel, B., Latreille, H., and Veron, J., *J. Catal.* **28**, 54 (1972).
9. Sayle, T. X. T., Parker, S. C., and Catlow, C. R. A., *J. Chem. Soc. Chem. Commun.*, 977 (1992).
10. Maitra, A. M., *Appl. Catal. A: General* **104**, 11 (1993).
11. Otsuka, K., Komatsu, T., and Shimizu, Y., *in* "Successful Design of Catalysts" (T. Inui, Ed.), p. 43. Elsevier, Amsterdam, 1988.
12. Doshi, R., Alcock, C. B., Gunasekaran, N., and Carberry, J. J., *J. Catal.* **140**, 557 (1993).
13. Spivey, J. J., *Ind. Eng. Chem. Res.* **26**, 2165 (1987).
14. Satterfield, C. N., "Heterogeneous Catalysis in Industrial Practice," 2nd ed. McGraw–Hill, New York, 1991.
15. Liu, W., and Flytzani-Stephanopoulos, M., *in* Armor, J. N., (Ed.), "Environmental Catalysis" (J. N. Armor, Ed.), ACS Symposium Series 552, p. 373. Am. Chem. Soc. Washington, DC, 1994.
16. Liu W., Sarofim, A. L., and Flytzani-Stephanopoulos, M., *Appl. Catal. B*, **4**, 167 (1994).
17. Liu, W., Sarofim, A. L., and Flytzani-Stephanopoulos, M., *in* "Materials and Processes for Environmental Protection," 1994 MRS Spring Meeting, San Francisco, CA, Paper I3.9.
18. Yao, H. C., and Yao, Y. F. Y., *J. Catal.* **86**, 254 (1984).
19. Pucci, A., (Ed.), "Catalysis and Automotive Pollution Control II." Elsevier Amsterdam, 1991.
20. Dow, W. P., and Huang, T. J., *J. Catal.* **147**, 322 (1994).
21. Frost, J. C., *Nature* **334**, 577 (1988)
22. Kim, D. J., *J. Am. Ceram. Soc.* **72**, 1415 (1989).
23. Levine, E. M., Robbins, C. R., and McMurdie, H. F., (Eds.), "Phase Diagrams for Ceramists." Am. Ceramic Soc. Westerville, OH, 1969.
24. Gerhardt-Anderson, R., and Nowick, A. S., *Solid State Ionics* **5**, 547 (1981).

25. Butler, V., Catlow, C. R. A., Fender, B. E. F., and Harding, J. H., *Solid State Ionics* **8**, 109 (1988).
26. Cullity, B. D., "Elements of X-ray Diffraction." Addison–Wesley, Reading, MA, 1978.
27. Liu, W., and Flytzani-Stephanopoulos, M., *J. Catal.* **153**, (1995).
28. Zhang, Y. P., Tao, S., Sarofim, A. F., and Flytzani-Stephanopoulos, M., *in* "NOx Reduction" (S. K. Agarwal, G. M. Marcelin, U. S. Ozkan, Eds.), ACS Symposium Series, Am. Chem. Soc. Washington, DC, Ch. XI, 1995, in press.
29. Wright, P. A., Natarajan, S., Thomas, J. M., and Gai-Boyes, P. L., *Chem. Mater.* **4**, 1053 (1992).
30. Choi, K. I., and Vannice, M. A., *J. Catal.* **131**, 22 (1991).
31. Rajadurai, S., and Carberry, J. J., *J. Catal.* **147**, 594 (1994).
32. Bond, G. C., and Namijo, S. N., *J. Catal.* **118**, 507 (1989).
33. Haruta, M., Tsubota, S., Kobayashi, T., Kageyma, H., Genet, M. J., and Delmon, B., *J. Catal.* **144**, 175 (1993).
34. Stephens, R. E., Hirschler, D. A., Jr., and Lamb, F. W., U.S. Patent 3 226 340, 1965.
35. Stiles, A. B., U. S. Patent 3 230 034, 1966.
36. Agudo, A. L., Palacios, J. M., Fierro, J. L. G., Laine, J., and Severio, F., *Appl. Catal. A: General* **91**, 43 (1992).
37. Voorhoeve, R. J. H., Remeika, J. P., Freeland, P. E., and Matthias, B. T., *Science* **177**, 353 (1972).
38. Schlatter, J. C., Klimisch, R. L., and Taylor, K. C., *Science* **179**, 798 (1973).
39. Voorhoeve, R. J. H., Johnson, D. W., Jr., Remeika, J. P., and Gallagher, P. K., *Science* **195**, 827 (1977).
40. Zwinkels, M. F. M., Jaras, S. G., and Menon, P. G., *Catal. Rev.-Sci. Eng.* **35**, 319 (1993).
41. Baiker, A., Marti, P. E., Keusch, P., Fritsch, E., and Reller, A., *J. Catal.* **146**, 268 (1994).
42. Klvana, D., Vaillancourt, J., Kirchnerova, J., and Chaouki, J., *Appl. Catal. A: General* **109**, 181 (1994).
43. Arai, H., Yamada, T., Eguchi, K., and Seiyama, T., *Appl. Catal.* **26**, 265 (1986).
44. Oh, S. H., Mitchell, P. J., and Siewert, R. M., *J. Catal.* **132**, 287 (1991).